Spin depolarization effect induced by charge state conversion of nitrogen vacancy center in diamond

Xiang-Dong Chen, Lei-Ming Zhou, Chang-Ling Zou, Cong-Cong Li, Yang Dong,
Fang-Wen Sun,[*] and Guang-Can Guo

Key Lab of Quantum Information, Chinese Academy of Sciences, School of Physics, University of Science and Technology of China,
Hefei 230026, People's Republic of China
and Synergetic Innovation Center of Quantum Information & Quantum Physics, University of Science and Technology of China,
Hefei 230026, People's Republic of China

The electron spin of the negatively charged the nitrogen vacancy center (NV^-) in diamond can be optically polarized through intersystem crossing, which enables the defect to be used for quantum computation and metrology. In this work, we studied the electron spin depolarization effect of the NV center induced by charge state conversion, which was proven to be a spin-independent process. The spin-state initialization fidelity was largely affected by the charge state conversion process. As a result, the optical polarization of the electron spin decreased about 14%(31%) with a high-power continuous-wave (pulsed) green laser. Moreover, the undefined fluorescence anomalous saturation effect of the NV center was analyzed and explained in detail based on the spin depolarization. The results demonstrated that a weak laser should be used for initialization of the NV center. In addition, the power and polarization of a laser for NV spin detection should be carefully adjusted to obtain the highest fluorescence signal. Our work also provided information that can increase the understanding of the charge state conversion and spin polarization processes of the NV center for quantum information and sensing.

I. INTRODUCTION

Due to stable fluorescence and long spin coherence time at room temperature [1,2], the negatively charged nitrogen vacancy (NV^-) center in diamond is a potential candidate for quantum computers [2–6], nanoscale sensors [7–9], and biological labeling [10]. The utilizing of NV^- electron spin includes initialization, manipulation, and detection processes. As high-fidelity initialization is the basis of the application with the NV center, it is very important to understand and optimize the optical polarization of the NV^- electron spin state. Usually a 532 nm off-resonant laser is used to pump the NV^- to an excited state, and then the spin-dependent intersystem crossing (ISC) will polarize the electron spin to the $m_s = 0$ sublevel in the ground state [11,12]. The reported spin state polarization probability varied from 42% to 96% [6,13–18], which was affected by the magnetic field, strain, and temperature [19–21]. The mechanism of optical spin polarization is not fully understood so far, and more experimental and theoretical studies are necessary [11,12,22,23].

Meanwhile, recent research has shown that optical pumping would also lead to the charge state conversion (CSC) of the NV center between neutral NV^0 and negative NV^- [18,24–27]. The power and wavelength dependence of the photon-induced CSC has been studied experimentally in earlier work [26–29]. Although a full understanding of the CSC has not been attained as of yet [20], it is widely accepted that the CSC is a two-photon process that occurs when the NV is pumped by a laser with a wavelength longer than 500 nm [26–29], and it is a single-photon process with a laser wavelength shorter than 450 nm [27,28]. The CSC of the NV center can be used for super-resolution microscopy [30–32] and spin state readout [33]. Moreover, the CSC changes the local

environment in diamond, which affects the results of quantum state manipulation [34,35]. Therefore, the CSC should be taken into consideration for NV-center-based quantum computation and metrology. However, the effect of CSC on spin state initialization and detection has not been studied systemically.

In this work, we studied experimentally the electron spin state depolarization effect with both single-photon and two-photon CSC. The photon-induced CSC process was proven to be spin-independent. Since a 532 nm laser was usually used for spin initialization and detection of the NV center, we measured the effect of two-photon CSC on electron spin optical polarization and detection in detail using a 532 nm laser. It was found in our experiment that the spin polarization dropped 14% with a high-power continuous-wave (CW) green laser, and 31% with a high-power pulsed green laser. Additionally, the anomalous saturation effect with regard to the fluorescence was studied and explained based on spin depolarization. The experimental results indicated that the initialization fidelity of the NV center could be improved by pumping the NV center with a low-power laser, and the power and polarization of the laser used for NV center spin detection should be carefully adjusted for the highest fluorescence signal. Our work can help to further the understanding of the optical dynamics of the NV center spin, which is important for both fundamental and application studies.

II. EXPERIMENTAL METHODS

The experiments were implemented at room temperature. The sample was a commercial chemical vapor deposition diamond plate with a [100] surface. The NV centers were produced by 20 keV ^{14}N ion implantation. A single NV center was identified by autocorrelation function measurement. As in Fig. 1(a), lasers with different wavelengths were combined by long pass dichroic mirrors (DMs), while the CW and pulsed green lasers were combined by polarizing beam splitters
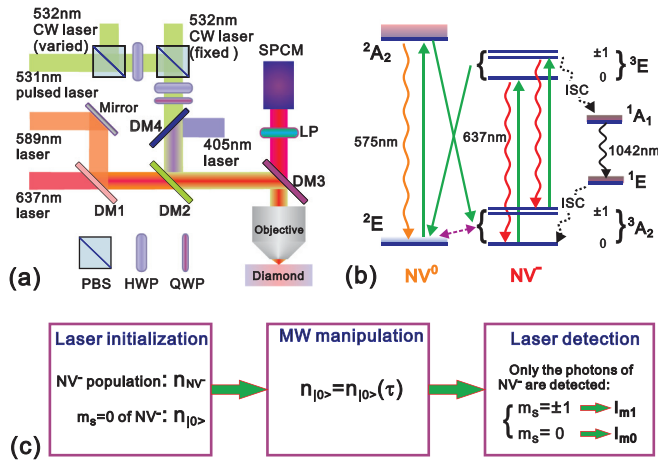
FIG. 1. (Color online) (a) Schematics of the experimental setup. LP, long pass filter; HWP, half-wave plate; QWP, quarter-wave plate; SPCM, single-photon counting modules. Four long pass dichroic mirrors were used: DM1, edge wavelength 605 nm; DM2, edge wavelength 536.8 nm; DM3, edge wavelength 658.8 nm; DM4, edge wavelength 506 nm. (b) Level structure of the NV center. The straight dashed arrows presented the single-photon CSC. The straight solid arrows were the transitions during two-photon CSC. The wavy dashed arrows indicated the nonradiative ISC transitions of NV⁻, while the wavy solid arrows indicated the spontaneous emission of the NV center. (c) The initialization-manipulation-detection process of the NV center as a spin qubit.

(PBSs). The lasers were switched by acousto-optic modulators and focused on a single NV center with a home-built confocal system. There were six lasers in the experiments. A 589 nm laser with low power was used to detect the charge state of NV [27,32]. A 637 nm laser was used to initialize the NV center to the NV⁰ charge state; this laser with low power and short duration was also applied for the polarization of the NV⁻ electron spin state without changing the charge state population. A 405 nm laser was used to study single-photon CSC. A CW 532 nm laser and a pulsed 531 nm laser with varied power were used to pump two-photon CSC. An additional CW 532 nm laser with fixed power (below saturation power) was used to locate the position of the NV center, and to detect the spin state of NV⁻. The microwave pulse was applied through a 15-μm-diam copper wire.

In this work, we considered only two charge states of the NV center, namely negative NV⁻ and neutral NV⁰ [Fig. 1(b)]. The fluorescence of NV⁰ shows a zero photon line (ZPL) at 575 nm, while the fluorescence of NV⁻ shows ZPLs at 637 (strong) and 1042 nm (weak) [36–38]. The ZPLs are accompanied by redshifted phonon sidebands. Only the photons from NV⁻ were detected in our experiment, while the photons from NV⁰ were blocked by a long pass filter with an edge wavelength of 668.9 nm. Therefore, the detected fluorescence intensity was linearly dependent on the NV⁻ population in our experiment. The precise charge state population of the NV center was obtained using the single-shot readout method [27,28]: the charge state was first initialized by a different pumping laser, and then a weak (μW) 589 nm laser was applied to detect the fluorescence intensity. The CSC process with the weak 589 nm laser was very slow, so that a sufficient number of photons

could be detected before the charge state was changed by the 589 nm laser. The photon count distribution was analyzed to determine the charge state population, where a higher photon count level meant NV⁻ and a lower level corresponded to NV⁰.

III. THE INITIALIZATION AND DETECTION OF NV⁻ ELECTRON SPIN

Application of the NV⁻ spin qubit usually requires implementation of the initialization-manipulation-detection process [Fig. 1(c)]. As shown in Fig. 1(b), the ground state $^3A_2$ and excited state ^3E of NV⁻ are spin triplet states, and the metastable states $^1A_1$ and ^1E are spin singlet states [23,37,39]. The zero-field splitting between $m_s = 0$ and ± 1 sublevels of the ground state $^3A_2$ is $D \approx 2\pi \times 2.87$ GHz at room temperature [38,40]. In our experiment, the spin states are equally populated at thermal equilibrium [41], as $k_B T / \hbar D > 10^3 (k_B$ denotes the Boltzmann constant and T is the temperature). Therefore, optical pumping is needed to change the NV center from unpolarized thermal equilibrium to a polarized state with high fidelity.

For the NV center, the ISC transitions with singlet states $^1A_1$ and ^1E are spin-selective processes. The ISC transitions between $^1A_1$ and ^3E with $m_s = \pm 1$ sublevels have a probability much larger than that with $m_s = 0$, and the ^1E singlet preferentially decays to the $m_s = 0$ sublevel in the ground state [9,14,20]. As a result, the whole ISC process ($^3E \rightarrow {}^1A_1 \rightarrow {}^1E \rightarrow {}^3A_2$) changes the electron spin state of NV⁻ from $m_s = \pm 1$ in the excited state to $m_s = 0$ in the ground state, with a total decay rate Γ. The lifetime of ^1E, which is around 180 ns at room temperature, is much longer than the lifetimes of $^1A_1$ and ^3E [42]. Therefore, the ISC rate Γ is mainly determined by the lifetime of ^1E, and it was measured to be about 5.5 μs^{-1} in our experiment. In addition to the spin polarization, the ISC transitions also result in the spin-dependent fluorescence of NV⁻, which is used for spin state readout [3,20].

As shown in Fig. 1(c), the optical initialization of the NV center can be depicted by the population of a negatively charged state (presented as n_{NV^-}) and the population of an $m_s = 0$ spin state of NV⁻ (presented as $n_{|0\rangle}$). After initialization, the electron spin state can be manipulated with a resonant microwave pulse. For the interaction of a two-level system with a single-mode resonant field, the time-revolution operator can be simply written as

$$U_I(\tau) = \begin{pmatrix} \cos\left(\frac{\Omega}{2}\tau\right) & i\sin\left(\frac{\Omega}{2}\tau\right) \\ i\sin\left(\frac{\Omega}{2}\tau\right) & \cos\left(\frac{\Omega}{2}\tau\right) \end{pmatrix}, \tag{1}$$

where Ω is the Rabi frequency and τ is the microwave duration. Applying the resonant microwave pulse on the transition between $m_s = 0$ and -1 sublevels in $^3A_2$, the Rabi oscillation is presented as the change of spin state population:

$$
\begin{aligned}
n_{|0\rangle}(\tau) &= n_{|0\rangle}(0)\cos^2\left(\frac{\Omega}{2}\tau\right) + n_{|-1\rangle}(0)\sin^2\left(\frac{\Omega}{2}\tau\right) \\
&= \frac{n_{NV^-}}{4}\left[1 + \frac{n_{|0\rangle}(0)}{n_{NV^-}} + \left(\frac{3n_{|0\rangle}(0)}{n_{NV^-}} - 1\right)\cos(\Omega\tau)\right].
\end{aligned}
\tag{2}
$$

The initial state of this Rabi oscillation is a mixed spin state. Due to the same ISC transition probability and

excited-state lifetime [9,14,19], the populations of $m_s = +1$ and -1 sublevels of NV$^-$ initialized by a laser have been assumed to be the same here ($n_{|+1\rangle}(0) = n_{|-1\rangle}(0) = \frac{n_{NV^-} - n_{|0\rangle}(0)}{2}$).

Assuming the detected fluorescence intensity with $m_s = 0(m_s = \pm1)$ of NV$^-$ is $I_{m0}(I_{m1})$, the difference between spin states would be $\delta_I = |I_{m0} - I_{m1}|$. According to the time-dependent part of Eq. (2), the amplitude of the electron spin Rabi oscillation signal is in proportion to $\frac{n_{NV^-}}{4}(\frac{3n_{|0\rangle}(0)}{n_{NV^-}} - 1)\delta_I$. Due to the hyperfine coupling between the electron spin of NV and the intrinsic ^{14}N nuclear spin [17,43], the microwave pulses in our experiment were nuclear spin-selective. In addition, as the intrinsic ^{14}N nuclear spin of NV was unpolarized here, the amplitude of the Rabi oscillation measured in our experiment was reduced to

$$A = \frac{1}{3} \times \frac{n_{NV^-}}{4}\left(\frac{3n_{|0\rangle}(0)}{n_{NV^-}} - 1\right)\delta_I = \frac{1}{4}R\delta_I. \quad (3)$$

Here, we have defined the optical initialization parameter $R = n_{NV^-}(\frac{n_{|0\rangle}}{n_{NV^-}} - \frac{1}{3})$. Therefore, as shown in Eq. (3), the detected amplitude of Rabi oscillation was determined by two factors: the NV center initialization (R) and the spin state detection (δ_I). To measure the initialization fidelity of the NV center, we kept the value of δ_I constant in the experiments, which was realized by fixing the power and duration of the laser for spin state detection. In the following sections, the change of Rabi oscillation amplitude A was directly used to present the change of optical initialization R. The parameter R includes two parts: the charge state initialization (n_{NV^-}) and the spin state initialization ($\frac{n_{|0\rangle}}{n_{NV^-}} - \frac{1}{3}$). With R and n_{NV^-} being measured in experiments, the spin polarization fidelity can be obtained as $\frac{R}{n_{NV^-}}$, which presents the difference between an optically polarized spin state and unpolarized thermal equilibrium.

IV. SPIN STATE DEPOLARIZATION DURING CHARGE STATE CONVERSION

The CSC of the NV center has been observed with a wide range of light illumination [26–28]. Usually, both ionization (NV$^-$ to NV^0) and recharging (NV^0 to NV$^-$) processes would be induced by the same laser. The NV$^-$ population of a steady state with laser excitation can be derived as $\frac{\gamma_r}{\gamma_i + \gamma_r}$ [32,44], where γ_i is the ionization rate and γ_r is the recharging rate. In our experiment, the highest NV$^-$ population [0.742(8), Fig. 2(a)] was obtained by 532 nm laser pumping, while the lowest NV$^-$ population [0.064(2), Fig. 2(b)] was obtained with a 637 nm laser.

A simple model in Fig. 1(b) was used to present the CSC process of the NV center. During the single-photon CSC, the NV center absorbs one photon and directly changes the charge state. The NV center will not be pumped to the excited states during the single-photon CSC. The two-photon CSC is more complicated because it has two separate steps. First, the NV center is pumped to the excited state of NV$^-$(^3E) or NV^0($^2A_2$) by absorbing one photon. Then, the charge state is changed by absorbing another photon [26,29,37]. Once the NV center is at the excited state ^3E, there are three possible transitions. In addition to the CSC, the NV center could also decay to the ground state of NV$^-$ through spontaneous radiation
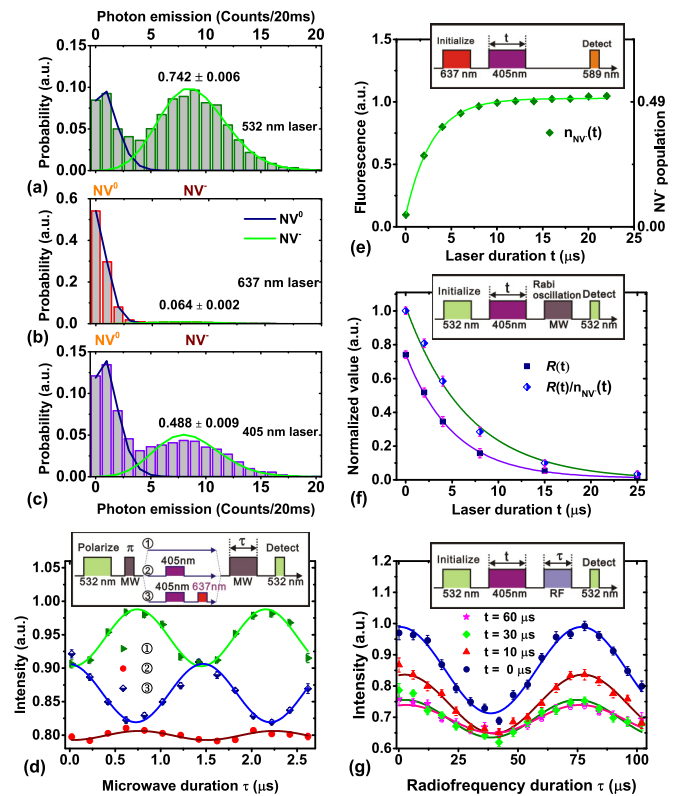

FIG. 2. (Color online) (a)–(c) The histograms of photon counts of a single NV center measured by the single-shot readout charge state method. The charge states were initialized by different lasers [a 0.6 mW 532 nm laser in (a), a 2 mW 637 nm laser in (b), and a 4 mW 405 nm laser in (c)], but detected by the same 589 nm laser with microwatt power. The solid lines are Poisson distribution fits. (d) Experiment results of NV$^-$ electron spin Rabi oscillation initialized by different lasers: ①, charge state and spin state initialized by 532 nm; ②, charge state and spin state initialized by 405 nm; ③, charge state initialized by a 405 nm laser and spin state initialized by a 637 nm laser. 405 nm laser: 30 μs duration, 1 mW power; 637 nm laser for spin polarization: 500 ns duration, 0.3 mW power; 532 nm initialization laser: 3 μs duration, 0.6 mW power; 532 nm detection laser: 300 ns duration, 0.6 mW power. (e) CSC process pumped by a 4 mW 405 nm laser. The fluorescence was detected by a 2 μs 0.27 mW 589 nm laser. The charge state was initialized by a 637 nm laser pulse with 5 μs duration and 6 mW power. (f) The electron spin polarization fidelity changed by a 4 mW 405 nm laser with different durations. (g) The nuclear spin Rabi oscillation was measured with different 405 nm pump laser durations. The power of the 405 nm laser was about 2 mW. The electron spin was fully depolarized with a 30 μs 405 nm laser in this situation.

or ISC transition. As mentioned before, the ISC transition will polarize the electron spin of NV$^-$ to an $m_s = 0$ state. Therefore, the two-photon CSC is accompanied by the spin state polarization process. The effect of pure CSC on the electron spin state should be obtained with single-photon CSC.

A. Spin-independent charge state conversion

A typical example of single-photon CSC was pumped by a 405 nm laser [28]. As shown in Fig. 2(d), the electron spin state was first prepared at $m_s = -1$ by green laser pumping and

subsequently a microwave π pulse; then different laser pulses were applied to change the optical initialization parameter R; finally, the Rabi oscillation was measured. We fixed the laser pulse for spin state detection. Therefore, the change of Rabi oscillation amplitude A was only caused by the optical initialization parameter R. In Fig. 2(d), R initialized by a 405 nm laser (② sequence) was much lower than that initialized by a 532 nm laser (① sequence). Here, the NV$^-$ population n_{NV^-} was between 0.742 [the steady-state population with a 532 nm laser, Fig. 2(a)] and 0.488 [the steady-state population with a 405 nm laser, Fig. 2(c)]. The change of charge state population was much lower than the change of R. The results proved that the electron spin state was depolarized by a 405 nm laser.

For comparison, a 0.3 mW 637 nm laser with 500 ns duration was applied after the 405 nm laser pulse [③ sequence in Fig. 2(d)]. As the CSC rate with the 0.3 mW 637 nm laser was much lower than 2 μs^{-1}, the short 637 nm laser pulse did not change the charge state population, but it can affect the spin state. The electron spin Rabi oscillation signal reappeared after applying the red laser pulse. The phase of Rabi oscillation with the ③ pulse sequence resulted in a different π from that with the ① and ② sequences. This indicated that the 637 nm laser polarized the electron spin state to $m_s = 0$, and it further proved that the decrease of R with the 405 nm laser was due to the depolarization of the electron spin state.

To analyze the relation between CSC and spin depolarization with a 405 nm laser, the CSC rate and spin depolarization rate were measured separately. The CSC rate was simply measured using the method in Fig. 2(e). The charge state of NV was first initialized to NV^0 by a 637 nm laser, then the 405 nm laser was applied with duration t, and the charge state was finally detected by a weak 589 nm laser. The duration of the 589 nm laser was carefully adjusted so that the spin state of NV$^-$ would be polarized by it, and the duration of that laser was not long enough to change the charge state initialized by the 405 nm laser. Therefore, the detected fluorescence intensity in Fig. 2(e) was mainly determined by the charge state population with 405 nm laser excitation. According to Eq. (A4), the 405 nm laser CSC rate $\gamma_c = \gamma_i + \gamma_r \approx 0.348(7)$ μs^{-1} was obtained by exponential fitting of the fluorescence in Fig. 2(e). The ionization rate can be obtained from γ_c and the steady-state NV$^-$ population as $\gamma_i = \gamma_c \times (1 - 0.488) \approx 0.177$ μs^{-1}.

The spin state depolarization rate of the 405 nm laser was obtained as shown in Fig. 2(f). The NV center was first initialized by the 532 nm laser. Then, a 405 nm laser with duration t was applied to change the charge state and the spin state. The electron spin Rabi oscillation was measured to obtained parameter $R(t)$. In Fig. 2(f), the decay rate of $R(t)$ [approximately 0.185(6) μs^{-1}] was very close to the photoionization rate in Fig. 2(e). This similarity was observed with different 405 nm laser powers. It strongly suggested that the CSC would lead to spin depolarization, as shown in Eq. (A5). The spin polarization fidelity in Fig. 2(f) was obtained as $\frac{R(t)}{n_{\text{NV}^-}(t)}$, where $n_{\text{NV}^-}(t) = 0.488 + (0.742 - 0.488)e^{-0.348 \ \mu\text{s}^{-1} \times t}$ was derived from Eq. (A4) [note that the CSC rate with the 405 nm laser was the same in Figs. 2(e) and 2(f), but the charge state populations were different]. The fully electron spin depolarization in Fig. 2(f) demonstrated that both the ionization and recharging processes of single-photon CSC were not spin-selective.

The polarization of the intrinsic ^{14}N nuclear spin of the NV center was also analyzed using single-photon CSC [Fig. 2(g)]. The nuclear spin was first initialized to $m_I = +1$ by 532 nm laser pumping with a 382 G external field [43]. Then, the 405 nm laser was applied to depolarize the electron spin state. The nuclear spin Rabi oscillation was observed by applying a resonant radiofrequency pulse. Due to the dipole interaction between nuclear spin and electron spin of the NV center, the results showed that CSC would also decrease the fidelity of nuclear spin manipulation. However, the nuclear spin Rabi oscillation signals still existed after the electron spin was fully depolarized. This indicated that the nuclear spin state was not directly affected by the CSC.

B. The power-dependent electron spin depolarization with two-photon charge state conversion

Although the spin depolarization effect induced by CSC has been demonstrated with a 405 nm laser, it is the 532 nm green laser that has been widely used for initialization and detection of the spin state of NV$^-$. The CSC pumped by a 532 nm laser is a two-photon process [27,28], where both spin polarization and depolarization effects should be considered. As mentioned before, the electron spin polarization process of NV$^-$ consists of two steps: optical pumping from a ground state to an excited state and the ISC transition through the singlet metastable states. The ISC transition does not require optical pumping, and it has a total transition rate $\Gamma \approx 5.5$ μs^{-1} in our experiment, as mentioned in Sec. III. Therefore, the spin polarization can be treated as a single-photon process. The contrast between the CSC transition rate (spin depolarization rate) and the electron spin polarization rate would be changed with laser power.

The spin state polarization process and the CSC process pumped by a CW 532 nm laser were measured with the pulse sequences shown in Figs. 3(a) and 3(b), respectively. In Fig. 3(a), the charge state was prepared at steady state with 532 nm laser excitation, and the spin state of NV$^-$ was prepared at $m_s = -1$. Another 532 nm laser pulse with duration t_s was applied to repolarize the electron spin state to $m_s = 0$. The detected fluorescence intensity would increase with t_s during the spin polarization process. The increased rate γ_s can be used to present the speed of spin polarization under 532 nm laser pumping. In contrast, the change of fluorescence with 532 nm duration t_c in Fig. 3(b) was caused by the CSC process, which was similar to Fig. 2(d). The CSC rate γ_c was obtained by exponentially fitting the fluorescence intensities with different durations of a 532 nm laser. The processes of spin polarization and CSC with different laser powers are shown in Figs. 3(c) and 3(d). It is worth noting that the ISC transition did not immediately stop after the 532 nm laser was turned off. Thus, the spin polarization rate was actually lower than γ_s in Fig. 3. However, in the weak excitation regime ($\gamma_s \leqslant \Gamma$), the spin polarization rate was very close to γ_s, and it can be presented by γ_s.

As shown in Fig. 3(e), the CSC rate increased much faster than the spin polarization rate. The ratio $\gamma_s : \gamma_c$ was about 68:1 with a 0.019 mW 532 nm CW laser, but the ratio became 3.6:1 with a 0.47 mW laser. In addition, the spin polarization rate in the strong excitation regime was limited by the ISC decay
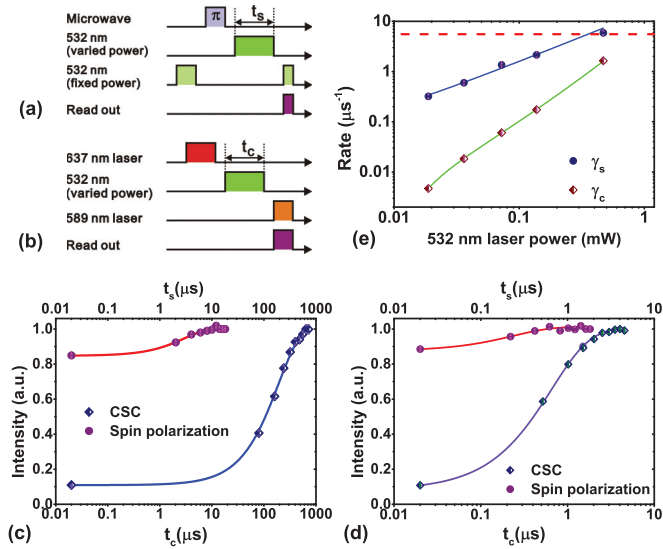
FIG. 3. (Color online) (a) and (b) Pulse sequences for the measurements of spin state polarization and CSC, respectively. t_s was the duration of the laser for spin polarization, and t_c was the duration of the laser for CSC. The 532 nm laser with fixed power (0.6 mW) in (a) was used for spin initialization (with 3 μs duration) and detection (with 0.3 μs duration). The 637 nm (for charge state initialization) and 589 nm (for charge state detection) lasers in (b) were the same as that in Fig. 2(e). (c) and (d) The measured fluorescence intensities changed with CW green laser durations of 0.019 and 0.47 mW CW, respectively. (e) The power dependence of the spin polarization rate (γ_s) and the CSC rate (γ_c). The rates were obtained by an exponential fit of the fluorescence variations during spin polarization and CSC, such as that in (c) and (d). The red dashed line presented the total ISC transition rate $\Gamma \approx 5.5\ \mu s^{-1}$ in our experiment.
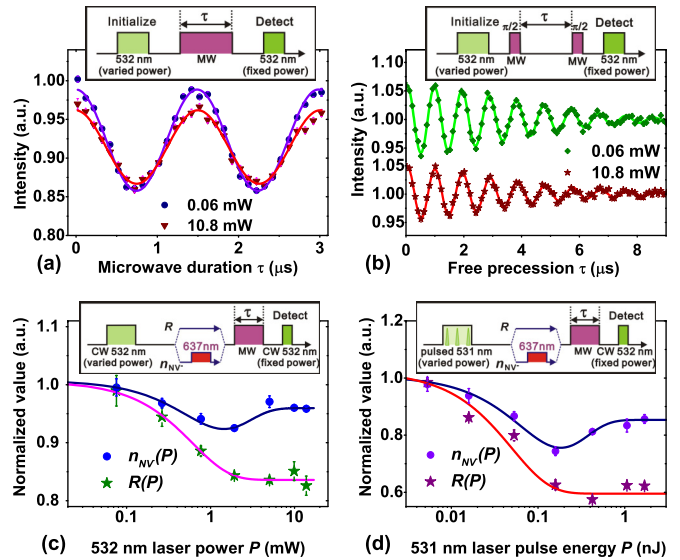

FIG. 4. (Color online) (a) and (b) Rabi oscillations and Ramsey fringes of the NV$^-$ electron spin state, respectively. The NV center was initialized by 532 nm lasers with different powers, and detected by the 532 nm laser with fixed power (0.6 mW, 0.3 μs duration). (c) and (d) The power dependence of polarization parameters initialized by a CW 532 nm laser and a pulsed 531 nm laser with a repetition rate of 5 MHz. A 637 nm laser for spin polarization: 0.3 mW power, 3 μs duration; a CW 532 nm laser for detection: 0.6 mW, 0.3 μs duration.

rate Γ. It can be expected that the spin state depolarization rate (CSC rate) would be much higher than the spin state polarization rate with ultrahigh-laser power.

Apparently, the total effect of laser excitation on the electron spin of NV$^-$ was determined by the contrast between the spin depolarization rate and the polarization rate. Therefore, the initialization fidelity of the NV$^-$ spin state should be changed with 532 nm laser power. In addition, the full depolarization effect of electron spin was supposed to be observed with the NV center initialized by a high-power 532 nm laser. In Figs. 4(a) and 4(b), we show the Rabi oscillation and Ramsey fringes of the NV$^-$ electron spin state initialized by a 0.06 and 10.8 mW 532 nm CW laser. The Rabi oscillation signal with the electron spin state initialized by a weak laser was larger than that initialized by a strong laser. This proved that the polarization fidelity of the NV$^-$ spin state decreased with the laser power. The spin coherence time was deduced from the decay of the Ramsey fringe envelope. The results showed that the electron spin coherence was not significantly changed with laser power.

The spin state initialization fidelity with a CW and a pulsed green laser was quantitatively analyzed as shown in Figs. 4(c) and 4(d). The parameter $R(P)$ initialized by a green laser with power P was obtained by measuring the Rabi oscillation of the electron spin state. Meanwhile, the NV$^-$ population $n_{NV^-}(P)$ initialized by a green laser can be

obtained using the single-shot charge state readout method, the results of which will be presented later. Here, for a complement of the single-shot readout method, we measured the power dependence of the NV$^-$ population in a different way. After the NV center was initialized by a 532 nm laser with various powers, we used a 637 nm laser pulse with fixed power and fixed width to pump the NV center. The duration of the 637 nm laser was carefully adjusted so that it repolarized the electron spin of NV$^-$ without significantly changing the charge state population. Therefore, the amplitude of electron spin Rabi oscillation measured with this pulse sequence was only determined by $n_{NV^-}(P)$ initialized with a 532 nm laser.

After the power dependence of $R(P)$ and $n_{NV^-}(P)$ was measured with Rabi oscillation, the power-dependent spin polarization fidelity was obtained as $\frac{R(P)}{n_{NV^-}(P)}$. As shown in Figs. 4(c) and 4(d), the spin polarization decreased 14(2)% with a high-power CW 532 nm laser, and 31(3)% with a high-power pulsed laser (5 MHz repetition rate). However, the exact value of spin polarization fidelity was not measured in our experiment.

C. The effect of intersystem crossing

The full depolarization effect of the spin state was not observed with two-photon CSC in the preceding section. This was because the microwave pulses were applied at least 500 ns after the laser pulse was turned off. A single ISC transition would repolarize the spin state of NV$^-$ before the Rabi oscillation was measured. Therefore, the measured spin depolarization effect in Fig. 4 was lower than that expected in Fig. 3.

In the pulsed laser experiment, the pulse width of the pulsed laser was about 78 ps, which was much shorter than the lifetimes of the excited states and the metastable states of NV^-. Therefore, the ISC transition during the laser pulse excitation can be neglected. For a single laser pulse with a fixed width, the spin depolarization effect induced by CSC would only be determined by the power of the laser. In contrast, the spin polarization effect of the ISC transition during the interval between two laser pulses was affected by the repetition rate of the pulsed laser. As a result, the effect of the whole pulse sequence would be changed with the repetition rate of the pulsed laser. The electron spin depolarization effect with the pulsed laser was larger than that with the CW laser, as shown in Fig. 4.

For a pulsed laser with a 5 MHz repetition rate in the experiment, the interval between two adjacent laser pulses was longer than the metastable states' lifetimes of NV^- [42]. The population of the metastable state can be treated as zero during the CSC process pumped by a laser pulse. Therefore, the full depolarization of the spin state during CSC with an ultrahigh-power pulsed laser can be presented as $\frac{R}{n_{NV^-}} = 0$. After the laser was turned off, a single ISC transition changed the spin state from $m_s = \pm 1$ to 0 with probability χ. Subsequently the spin polarization effect became $\frac{R}{n_{NV^-}} = \frac{2\chi}{3}$. In Fig. 4(d), we found that $\frac{R}{n_{NV^-}}$ initialized by an ultrahigh-power laser was about 69% of the maximum value [$(\frac{R}{n_{NV^-}})_{max} \lesssim \frac{2}{3}$]. Therefore, the polarization probability of a single ISC transition was estimated to be $\chi \lesssim 69\%$.

V. THE FLUORESCENCE ANOMALOUS SATURATION

As the fluorescence intensity varied with electron spin, it was expected that the spin depolarization induced by CSC should also affect the emission of the NV center. In fact, the fluorescence anomalous saturation effect of the NV center, presented as the decrease of fluorescence intensity with laser power, has been observed for a long time [45–47]. In Ref. [46], Chapman *et al.* analyzed the anomalous saturation of the NV center with different external magnetic fields, and they suggested that the anomalous saturation was caused by the electron spin depolarization of NV^-, although the reason for the depolarization was not clearly specified. However, in Ref. [47], Han *et al.* deduced that the anomalous saturation resulted from the power dependence of the dark state population.

In Figs. 5(a) and 5(b), we measured the power-dependent fluorescence intensity and charge state population with a green laser. For both a CW laser and a pulsed laser, the NV center fluorescence showed a decrease with laser power in the strong excitation regime, as expected. The population of NV^0 (as a dark state here) did not increase with laser power in the strong excitation regime. Instead, the depolarization effect of the electron spin state [Figs. 4(c) and 4(d)] fitted the tendency of anomalous saturation. The results supported the assumption that the anomalous saturation effect was induced by the spin depolarization, which was proven to result from CSC in the strong excitation regime. Actually, the increase of the NV^- population in the high-power regime might also be caused by the spin state depolarization effect [28].
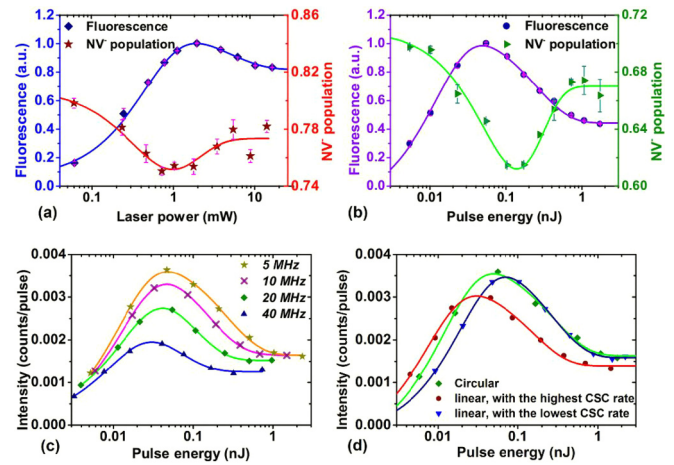

FIG. 5. (Color online) The power-dependent fluorescence intensity and charge state population with (a) 532 nm CW laser and (b) 531 nm pulsed laser with a repetition rate of 5 MHz. The charge state population was detected by the single-shot charge state readout method. (c) The anomalous saturation of the NV center with different repetition rates of pulsed laser. The lasers were circularly polarized, with repetition rates ranging from 5 to 40 MHz. (d) The fluorescence saturation effect of the single NV center with different laser polarizations. The repetition rate of the pulsed laser was 5 MHz.

The fluorescence anomalous saturation effect also changed with the repetition rate of the pulsed laser, as shown in Fig. 5(c). Unlike the Rabi oscillation measurement, the spontaneous emission was measured right after the laser pulse was turned off (the lifetime of the excited state ^3E was 10−15 ns in our experiment). The ISC transition cannot repolarize the spin state before spontaneous emission is measured. Therefore, the full spin depolarization can be observed through the anomalous saturation effect. For the results of a pulsed laser with a repetition rate of 5 MHz, the saturated fluorescence intensity was about 43% of the maximum intensity. Considering the change of charge state population with laser power, the results indicated that the spontaneous emission intensity with a fully depolarized spin state was lower than 42% of the spontaneous emission with a polarized spin state, $m_s = 0$.

As the two-photon CSC rate was also changed with the polarization of the laser [32,34], we observed different anomalous saturation effects of the NV center with different laser polarizations, as shown in Fig. 5(d). The results showed that the highest fluorescence intensity of the NV center in [100] diamond was obtained with a circular polarization laser. This demonstrated that the power and polarization of the laser should be carefully chosen for the maximum fluorescence intensity of the NV center. In addition, a fast CSC transition should be avoided during spin state detection.

VI. DISCUSSION AND CONCLUSIONS

Usually, the optical initialization and detection of the NV center is performed with a 532 nm CW laser. However, our experiment demonstrated that optical pumping can actually lead to electron spin depolarization. As a result, the spin polarization fidelity decreased with 532 nm laser power. In previous experiments, electron spin polarization and detection

were realized with the same laser, and the power was usually larger than the fluorescence saturation power (where the fluorescence intensity was half of the maximum fluorescence intensity) [2,46]. The results in Fig. 4(c) showed that the electron spin polarization and NV$^-$ population initialized by a CW 532 nm laser with saturation power (approximately 0.24 mW) was lower than the maximum value. Therefore, a weak 532 nm laser was needed for high-fidelity NV$^-$ initialization. On the other hand, the laser used for fluorescence detection should be carefully adjusted according to the anomalous saturation effect. To improve the performance of the NV center as a spin qubit, two lasers with different powers should be applied separately for NV center initialization and detection.

In summary, we experimentally studied the effect of CSC on the initialization and detection of NV center electron spin. The spin state depolarization effect was observed with both single-photon and two-photon CSC processes. The CSC was proven to be spin-independent. As a 532 nm laser was usually used for NV center initialization and detection, we found that the electron spin polarization dropped 14% with a high-power CW green laser and 31% with a high-power pulsed green laser. The results indicated that the high-fidelity spin polarization of the NV center should be obtained with weak laser pumping. Due to spin depolarization induced by CSC, the fluorescence anomalous saturation effect of the NV center was also observed and analyzed in the experiment. It demonstrated that the laser for detecting the NV center should be carefully chosen to avoid the depolarization effect of the electron spin. The results can help to further the understanding of the CSC and spin state polarization processes of the NV center, and to develop applications of the NV center for quantum computation and metrology.

APPENDIX: THE CHARGE STATE CONVERSION RATE AND THE SPIN DEPOLARIZATION RATE

The CSC can be treated as the transition between the bound state and the continuum state. It is reasonable to assume that the CSC is spin-independent. Then, the rate equations for single-photon CSC could be written as

$$\frac{d}{dt}n_{|0\rangle} = -\gamma_i n_{|0\rangle} + \frac{\gamma_r}{3}n_{NV^0}, \tag{A1}$$

$$\frac{d}{dt}n_{|\pm1\rangle} = -\gamma_i n_{|\pm1\rangle} + \frac{\gamma_r}{3}n_{NV^0}, \tag{A2}$$

$$\frac{d}{dt}n_{NV^0} = \gamma_i(n_{|0\rangle} + n_{|+1\rangle} + n_{|-1\rangle}) - \gamma_r n_{NV^0}. \tag{A3}$$

Here, $n_{|0\rangle,|\pm1\rangle}$ denotes the population of NV$^-$ with spin state $m_s = 0, \pm1$. n_{NV^0} is the population of NV^0. The neutral charge state population during the CSC is solved as

$$n_{NV^0}(t) = \frac{\gamma_i}{\gamma_i + \gamma_r} + \left(n_{NV^0}(0) - \frac{\gamma_i}{\gamma_i + \gamma_r}\right)e^{-(\gamma_i+\gamma_r)t}, \tag{A4}$$

where t is the duration of the laser. It shows that the charge state population changes with rate $\gamma_c = \gamma_i + \gamma_r$, and the steady-state population of NV^0 is presented as $\frac{\gamma_i}{\gamma_i+\gamma_r}$. The population of NV$^-$ can be obtained as $n_{NV^-} = 1 - n_{NV^0}$. The spin state depolarization effect is also solved as

$$\frac{d}{dt}(n_{|0\rangle} - n_{|\pm1\rangle}) = -\gamma_i(n_{|0\rangle} - n_{|\pm1\rangle}). \tag{A5}$$

The population difference between different spin states can be written as $n_{|0\rangle} - n_{|\pm1\rangle} = \frac{3}{2}R$, where R is defined in Eq. (3).

Normally, the two-photon CSC is more complicated than the single-photon process, and it cannot be depicted by Eqs. (A1)–(A3), as the ISC transition should be considered. But for the pulsed laser used in our experiment, the pulse width was much shorter than the lifetime of NV excited states and metastable states [42]. Therefore, the spontaneous decay and nonradiative ISC transition of the NV center can be neglected during the laser pumping. The two-photon CSC with a pulsed laser can also be analyzed by Eqs. (A1)–(A3).

[1] G. Balasubramanian, P. Neumann, D. Twitchen, M. Markham, R. Kolesov, N. Mizuochi, J. Isoya, J. Achard, J. Beck, J. Tissler *et al.*, Nat. Mater. **8**, 383 (2009).

[2] P. C. Maurer, G. Kucsko, C. Latta, L. Jiang, N. Y. Yao, S. D. Bennett, F. Pastawski, D. Hunger, N. Chisholm, M. Markham *et al.*, Science **336**, 1283 (2012).

[3] F. Jelezko, T. Gaebel, I. Popa, A. Gruber, and J. Wrachtrup, Phys. Rev. Lett. **92**, 076401 (2004).

[4] P. Neumann, N. Mizuochi, F. Rempp, P. Hemmer, H. Watanabe, S. Yamasaki, V. Jacques, T. Gaebel, F. Jelezko, and J. Wrachtrup, Science **320**, 1326 (2008).

[5] E. Togan, Y. Chu, A. Trifonov, L. Jiang, J. Maze, L. Childress, M. Dutt, A. Sørensen, P. Hemmer, A. Zibrov *et al.*, Nature (London) **466**, 730 (2010).

[6] P. Neumann, R. Kolesov, B. Naydenov, J. Beck, F. Rempp, M. Steiner, V. Jacques, G. Balasubramanian, M. L. Markham, D. J. Twitchen *et al.*, Nat. Phys. **6**, 249 (2010).

[7] G. Balasubramanian, I. Y. Chan, R. Kolesov, M. Al-Hmoud, J. Tisler, C. Shin, C. Kim, A. Wojcik, P. R.Hemmer, A. Krueger *et al.*, Nature (London) **455**, 648 (2008).

[8] J. R. Maze, P. L. Stanwix, J. S. Hodges, S. Hong, J. M. Taylor, P. Capperllaro, L. Jiang, M. Dutt, E. Togan, A. S. Zibrov *et al.*, Nature (London) **455**, 644 (2008).

[9] L. Rondin, J.-P. Tetienne, T. Hingant, J.-F. Roch, P. Maletinsky, and V. Jacques, Rep. Prog. Phys. **77**, 056503 (2014).

[10] L. P. McGuinness, Y. Yan, A. Stacey, D. A. Simpson, L. T. Hall, D. Maclaurin, S. Prawer, P. Mulvaney, J. Wrachtrup, F. Caruso *et al.*, Nat. Nano. **6**, 358 (2011).

[11] N. B. Manson, J. P. Harrison, and M. J. Sellars, Phys. Rev. B **74**, 104303 (2006).

[12] P. Delaney, J. C. Greer, and J. A. Larsson, Nano Lett. **10**, 610 (2010).

[13] G. Waldherr, Y. Wang, S. Zaiser, M. Jamali, T. S. Herbruggen, H. Abe, T. Ohshima, J. Isoya, J. F. Du, P. Neumann *et al.*, Nature (London) **506**, 204 (2014).

[14] L. Robledo, H. Bernien, T. van der Sar, and R. Hanson, New J. Phys. **13**, 025013 (2011).

[15] J. Harrison, M. Sellars, and N. Manson, Diamond Relat. Mater. **15**, 586 (2006).

[16] F. Jelezko, T. Gaebel, I. Popa, M. Domhan, A. Gruber, and J. Wrachtrup, Phys. Rev. Lett. **93**, 130501 (2004).

[17] S. Felton, A. M. Edmonds, M. E. Newton, P. M. Martineau, D. Fisher, D. J. Twitchen, and J. M. Baker, Phys. Rev. B **79**, 075203 (2009).

[18] G. Waldherr, J. Beck, M. Steiner, P. Neumann, A. Gali, T. Frauenheim, F. Jelezko, and J. Wrachtrup, Phys. Rev. Lett. **106**, 157601 (2011).

[19] D. M. Toyli, D. J. Christle, A. Alkauskas, B. B. Buckley, C. G. Van de Walle, and D. D. Awschalom, Phys. Rev. X **2**, 031001 (2012).

[20] M. W. Doherty, N. B. Manson, P. Delaney, F. Jelezko, J. Wrachtrup, and L. C. Hollenberg, Phys. Rep. **528**, 1 (2013).

[21] M. W. Doherty, V. V. Struzhkin, D. A. Simpson, L. P. McGuinness, Y. Meng, A. Stacey, T. J. Karle, R. J. Hemley, N. B. Manson, L. C. L. Hollenberg *et al.*, Phys. Rev. Lett. **112**, 047601 (2014).

[22] S. K. Choi, M. Jain, and S. G. Louie, Phys. Rev. B **86**, 041202 (2012).

[23] M. L. Goldman, M. W. Doherty, A. Sipahigil, N. Y. Yao, S. D. Bennett, N. B. Manson, A. Kubanek, and M. D. Lukin, Phys. Rev. B **91**, 165201 (2015).

[24] T. Gaebel, M. Domhan, C. Wittmann, I. Popa, F. Jelezko, J. Rabeau, A. Greentree, S. Prawer, E. Trajkov, P. R. Hemmer *et al.*, Appl. Phys. B **82**, 243 (2006).

[25] N. B. Manson and J. P. Harrison, Diamond Relat. Mater. **14**, 1705 (2005).

[26] K. Beha, A. Batalov, N. B. Manson, R. Bratschitsch, and A. Leitenstorfer, Phys. Rev. Lett. **109**, 097404 (2012).

[27] N. Aslam, G. Waldherr, P. Neumann, F. Jelezko, and J. Wrachtrup, New J. Phys. **15**, 013064 (2013).

[28] X.-D. Chen, C.-L. Zou, F.-W. Sun, and G.-C. Guo, Appl. Phys. Lett. **103**, 013112 (2013).

[29] P. Siyushev, H. Pinto, M. Vörös, A. Gali, F. Jelezko, and J. Wrachtrup, Phys. Rev. Lett. **110**, 167402 (2013).

[30] K. Y. Han, S. K. Kim, C. Eggeling, and S. W. Hell, Nano Lett. **10**, 3199 (2010).

[31] M. Pfender, N. Aslam, G. Waldherr, P. Neumann, and J. Wrachtrup, Proc. Natl. Acad. Sci. USA **111**, 14669 (2014).

[32] X. Chen, C. Zou, Z. Gong, C. Dong, G. Guo, and F. Sun, Light: Sci. Appl. **4**, e230 (2015).

[33] B. J. Shields, Q. P. Unterreithmeier, N. P. de Leon, H. Park, and M. D. Lukin, Phys. Rev. Lett. **114**, 136402 (2015).

[34] F. Dolde, M. W. Doherty, J. Michl, I. Jakobi, B. Naydenov, S. Pezzagna, J. Meijer, P. Neumann, F. Jelezko, N. B. Manson *et al.*, Phys. Rev. Lett. **112**, 097603 (2014).

[35] G. Waldherr, P. Neumann, S. F. Huelga, F. Jelezko, and J. Wrachtrup, Phys. Rev. Lett. **107**, 090401 (2011).

[36] P. Kehayias, M. W. Doherty, D. English, R. Fischer, A. Jarmola, K. Jensen, N. Leefer, P. Hemmer, N. B. Manson, and D. Budker, Phys. Rev. B **88**, 165202 (2013).

[37] N. B. Manson, K. Beha, A. Batalov, L. J. Rogers, M. W. Doherty, R. Bratschitsch, and A. Leitenstorfer, Phys. Rev. B **87**, 155209 (2013).

[38] X.-D. Chen, C.-H. Dong, F.-W. Sun, C.-L. Zou, J.-M. Cui, Z.-F. Han, and G.-C. Guo, Appl. Phys. Lett. **99**, 161903 (2011).

[39] K. Jensen, N. Leefer, A. Jarmola, Y. Dumeige, V. M. Acosta, P. Kehayias, B. Patton, and D. Budker, Phys. Rev. Lett. **112**, 160802 (2014).

[40] V. M. Acosta, E. Bauch, M. P. Ledbetter, A. Waxman, L. S. Bouchard, and D. Budker, Phys. Rev. Lett. **104**, 070801 (2010).

[41] F. Kaiser, V. Jacques, A. Batalov, P. Siyushev, F. Jelezko, and J. Wrachtrup, arXiv:0906.3426 (quant-ph).

[42] V. M. Acosta, A. Jarmola, E. Bauch, and D. Budker, Phys. Rev. B **82**, 201202 (2010).

[43] V. Jacques, P. Neumann, J. Beck, M. Markham, D. Twitchen, J. Meijer, F. Kaiser, G. Balasubramanian, F. Jelezko, and J. Wrachtrup, Phys. Rev. Lett. **102**, 057403 (2009).

[44] Y. Doi, T. Makino, H. Kato, D. Takeuchi, M. Ogura, H. Okushi, H. Morishita, T. Tashima, S. Miwa, S. Yamasaki *et al.*, Phys. Rev. X **4**, 011057 (2014).

[45] T. Plakhotnik and R. Chapman, New J. Phys. **13**, 045001 (2011).

[46] R. Chapman and T. Plakhotnik, Phys. Rev. B **86**, 045204 (2012).

[47] K. Y. Han, D. Wildanger, E. Rittweger, J. Meijer, S. Pezzagna, S. W. Hell, and C. Eggeling, New J. Phys. **14**, 123002 (2012).